Materials & Design 207 (2021) 109846

Contents lists available at ScienceDirect

Materials & Design

journal homepage: www.elsevier.com/locate/matdes

Stability-limited ion-exchange of calcium with zinc in biomimetic hydroxyapatite

Mark M.J. van Rijt [a,1], Sjoerd W. Nooteboom [a,1], Arno van der Weijden [b], Willem L. Noorduin [b], Gijsbertus de With [a,*]

[a] Laboratory of Physical Chemistry, Centre for Multiscale Electron Microscopy, Department of Chemical Engineering and Chemistry, Eindhoven University of Technology, P.O. Box 513, 5600 MB Eindhoven, The Netherlands
[b] AMOLF, 1098 XG Amsterdam, The Netherlands

HIGHLIGHTS

- 16% of Ca^{2+} ions in hydroxyapatite can be exchanged with Zn^{2+} ions within 10 s.
- At ~20 % Zinc incorporation, hydroxyapatite crystals start to gradually dissolve.
- Dissolved hydroxyapatite products and Zn^{2+} ions react to form hopeite .
- Exchange experiments on TEM grids allow for rapid analysis with μL sample volumes.

GRAPHICAL ABSTRACT

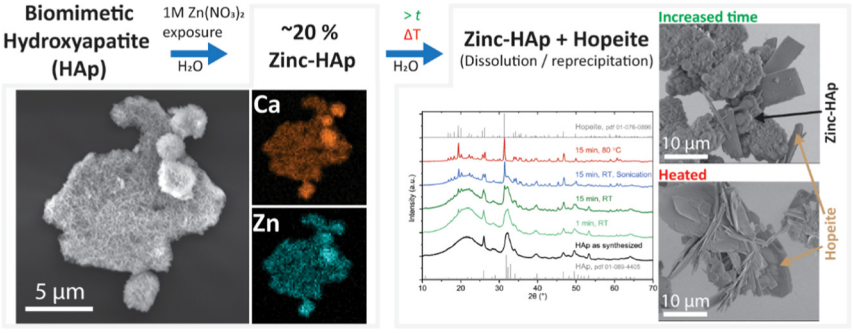

ARTICLE INFO

Article history:
Received 12 January 2021
Revised 20 May 2021
Accepted 21 May 2021
Available online 23 May 2021

Keywords:
Ion-exchange
Hydroxyapatite
HAp
Calcium
Zinc

ABSTRACT

The exchange of Ca^{2+} ions in hydroxyapatite (HAp) with Zn^{2+} ions into Zn-HAp is of interest for applications ranging from bone tissue engineering to the use as a precursor in subsequent ion-exchange reactions. Previous studies, using direct synthesis, showed that ~ 20 mol% Zn^{2+} ions can be incorporated into HAp, before byproducts are observed. However, this is realized at the cost of a loss in crystallinity and control over crystal size and shape with increasing amounts of Zn^{2+} ion incorporation. In this work a simple post-synthetic ion-exchange strategy for the formation of Zn-HAp has been investigated. By merely exposing HAp to high concentrations of zinc nitrate in water, up to 22 mol% of the Ca^{2+} ions can displaced by Zn^{2+} ions without any measured loss in crystallinity and preservation of crystallite size and shape. It was found that the incorporation of Zn^{2+} ions destabilizes the HAp crystals resulting in their gradual dissolution and reprecipitation. Consequently, promoting the exchange of Ca^{2+} with Zn^{2+}ions using increased reaction times, sonication and increased temperature results in an increased dissolution of HAp and precipitation of hopeite crystals, thereby preventing the formation of more zinc rich Zn-HAp.

1. Introduction

Hydroxyapatite (HAp, $Ca_{10}(PO_4)_6(OH)_2$) is one of the most abundant minerals in biology. In both bone and teeth HAp is mineralized *intra* and *inter* fibrillary in collagen providing strength to these materials [1,2], a strategy that could be used to advantage in additive manufacturing [3]. Synthetically highly crystalline HAp can be formed in dispersion [4], although biological HAp is rather ill-defined [5]. While HAp is the naturally occurring mineral in collagen [6], collagen has thus far only been mineralized to a limited extent via direct synthesis [7] with other materials includ-

* Corresponding author.
E-mail address: G.deWith@TUe.nl (G. de With).
[1] Contributed equally.

https://doi.org/10.1016/j.matdes.2021.109846
0264-1275/

ing calcium carbonate [8], silica [9], yttria-stabilized zirconia [10] and iron oxides [11].

To extend the range of materials that can be incorporated into collagen and other organic templates, an alternative strategy would be the use of ion-exchange [12–14]. The preservation of crystallite shape and location, important for providing toughness and strength [15,16], should allow for a post-synthetic ion-exchange of the mineral inside the template, avoiding the need to investigate new mineralization protocols but still being able to introduce new properties [17]. The substitution of both PO_4^{3-} and Ca^{2+} ions in HAp with a range of respective anions and cations is possible [18]. However, the relatively high lattice energy of HAp and apatite species in general will make anion exchange challenging [13,19–21]. The substitution of Ca^{2+} ions with Zn^{2+} ions (further on referred to as Ca and Zn), leading to Zn-HAp, has been investigated for a range of applications including (antimicrobial) coatings [22–24], dental applications [25], drug or DNA delivery [26,27], bone tissue engineering [28–30], improvement in bio-activity and selective protein adsorption [31,32]. By substituting Ca with Zn during HAp synthesis 15 – 20 mol% of the Ca could be replaced with Zn [25,28,33–35]. Increasing the amount of Zn in the reaction medium results in a progressive increase in Zn substitution, but with an associated decrease in crystallinity and control over the crystal size and shape [25,33]. Furthermore increasing the concentration of Zn in the reaction medium above 15 – 20 mol% leads to the undesired formation of $CaZn_2(PO_4)_2{\cdot}H_2O$ [28,34,35] and $Zn_3(PO_4)_2{\cdot}2H_2O$ (hopeite) [34].

Apart from its use as an heavy metal remover as e.g. discussed by Oliva et al.[36], substituting Ca by Zn via post-synthetic ion-exchange for the specific goal of obtaining Zn-HAp has received limited attention. Hayakawa et al. [31] exposed HAp to up to 11.5 mM of aqueous $Zn(NO)_3$ solutions for 24 h at 80 °C and they exchanged 2.3 mol% of Ca with Zn without loss in crystallinity. Wang et al. [37] exposed a HAp slurry to 1 M $Zn(NO)_3$ solution for 7 days at 37 °C resulting in a 9.5 mol% exchange of Ca with Zn for HAp with the formation of β-tricalcium phosphate as a byproduct. Using organic solvents, Chen et al. [38] were able to incorporate a range of cations in HAp including Zn. A maximum of 20.5 mol% could be exchanged in the case of iron [38]. These processes generally result in a very limited Zn incorporation of less than 20 mol%, require significantly longer than 24 h reaction times or need to be performed in organic solvents.

Here ion-exchange [13,14] of Ca with Zn in HAp to Zn-HAp in an aqueous dispersion was investigated by a combination of fast screening experiments, directly performed on TEM grids, in combination with more traditional ion-exchange experiments on dispersed HAp powders. Exposing synthetic HAp to a significant concentration of $Zn(NO_3)_2$, it was found that ~ 20 mol% of Ca can be exchanged with Zn within a minute while preserving morphology and crystallinity. Further promoting the incorporation of Zn into Zn-HAp by using increased exposure time or increased temperature only results in a minimal increase in incorporated Zn. The main reason for this seems to be the destabilizing effect of the Zn incorporated into the HAp crystals close to 20 mol%. This causes the gradual dissolution of the Zn-HAp crystals, followed by the precipitation of hopeite. Nevertheless, the method used leads to the rapid incorporation of what seems to be the maximum of Zn in HAp.

2. Experimental

2.1. Synthesis of hydroxyapatite nanoplatelets

HAp nanoplatelets were synthesized according to the procedure described by Habraken et al.[4] A buffer solution was prepared by dissolving 50 mM Trizma base and 150 mM NaCl in pure water. The pH was set to 7.4 using concentrated HCl solution. Phosphate and calcium stock solutions were prepared by adding either 10 mM K_2HPO_4 or $CaCl_2$ to the buffer solution. Both stock solutions were set to pH 7.4 by dropwise addition of 0.1 M HCl or NaOH. The reaction was initiated by adding phosphate stock solution to calcium stock solution in a ratio of 0.7:1.0 in a beaker. The reaction mixture was stirred for at least 4 h depending on volume under magnetic stirring. The HAp nanoplatelets were isolated by centrifugation using either an Optima L-90 K ultracentrifuge equipped with a Type 70 Ti rotor at 20,000 rpm for 20 min or an Eppendorf MiniSpinPlus equipped with a F-45–12-11 rotor at 14,500 rpm for 15 min. The so-obtained pellets were redispersed in pure water followed by another centrifugation step. This procedure was performed twice. After centrifugation the product was dried overnight at 60 °C.

2.2. On-grid grid ion-exchange experiments

Several mg of HAp was dispersed in pure water and 10 μL of the resulting HAp dispersion was placed on a glow discharged continuous carbon Au grid for 40 s. The droplet was removed by manual blotting using a filter paper. The pH of the $Zn(NO_3)_2{\cdot}6H_2O$ ion-exchange solution was preadjusted by dropwise addition of 0.1 M nitric acid. For RT experiments a HAp-loaded grid was placed on a 300 μL droplet of $Zn(NO_3)_2{\cdot}6H_2O$ solution for the targeted amount of time. For on-grid exchange at higher temperature, a HAp loaded grid was submerged vertically using Teflon coated tweezers for the targeted amount of time in a preheated $Zn(NO_3)_2{\cdot}6H_2O$ solution. After either ion-exchange reaction procedure, excess Zn was removed by washing in freshly prepared acetone and pure water (twice).

2.3. Powder ion-exchange experiments

For ion-exchange on HAp powder, > 10 mg of HAp was dispersed in 1 mL of pure-water, which was injected in fluent motion into 15 mL of 1 M $Zn(NO_3)_2{\cdot}6H_2O$ solution. For short reactions (less than 1 min) the dispersion was dispersed by shaking. For reactions longer than 1 min the dispersion was either stirred or sonicated (the latter at room temperature only) to prevent sedimentation. After the 1 to 15 min reaction time (and cooling on an ice bath in case of heated reactions), the powder was purified and dried by centrifugation, similar to as during the synthesis of HAp, or by rapid filtration over a GE Whatman^{tm} 7 μm filter paper.

2.4. Analysis

pH measurements were performed using a Metrohm (6.0234.100) 125 mm unitrode pH probe.

Scanning Electron Microscopy (SEM) and Energy Dispersive X-ray (EDX) measurements were conducted using either a Phenom ProX (Thermo Fischer Scientific, TFS) operated at 5 kV (for imaging) using a backscattering detector and at 15 kV (for EDX mapping) or on a Verios 460 (TFS) operated at 5 kV and 100 pA (for imaging) using a circular Everhart-Thornley backscatter detector at 30 kV (for EDX analysis). Elemental quantification was performed using the built-in Phenom software or AZtec 2.4, respectively, based on internal device calibrations. For every reaction condition at least 5 different areas were mapped using EDX. Regular SEM imaging was conducted using a Quanta 3D (TFS) operated at 5.0 kV which was equipped with a field emission gun and an ETL secondary electron detector.

Transmission Electron Microscopy (TEM) and Selected Area Electron Diffraction (SAED) images were collected on a Tecnai

T20 (TFS) operated at 200 kV, equipped with a 4096 × 4096 pixels CETA CMOS camera.

Size analysis of the HAp particles was performed by judiciously choosing representative particles in representative images, and measuring their length, width and thickness manually using an in-house Matlab script.

Powder X-ray difraction (pXRD) measurements were performed on a MiniFlex 600 difractometer operated at 40 kV and 15 mA using Cu Kα radiation. Automatic peak assignments were made by the PDXL 2 software.

Cryogenic transmission electron microscopy (CryoTEM) samples were prepared by depositing 3 μL of a dispersion on a 200 mesh Au grid covered with a Quantifoil R 2/2 holey carbon films (QuantifoilMicro Tools GmbH, part of SPT Life Sciences group). An automated vitrification robot (TFS, Vitrobot Mark III) was used for blotting and plunging in liquid ethane. All TEM grids were surface plasma treated for 40 s using a Cressington 208 carbon coater prior to use.

CryoTEM studies were performed on the TU/e cryoTITAN (TFS) equipped with a field emission gun (FEG), a postcolumn Gatan Energy Filter (model 2002) and a post-GIF 2 k × 2 k Gatan CCD camera (model 794). The microscope was operated at 300 kV acceleration voltage in bright field mode and with zero-loss energy filtering.

3. Results

3.1. Incorporation of Zn into HAp

Ion-exchange was performed by exposing HAp to a 1 M Zn $(NO_3)_2{\cdot}6H_2O$ solution set to pH 2.9 by adding 0.1 M nitric acid. To rapidly probe the incorporation of Zn into HAp, HAp-coated continuous carbon TEM grids were floated on a droplet of Zn $(NO_3)_2$ solution for 1 min, followed by washing (*Experimental*). SEM imaging showed the presence of clusters of HAp before and after the reaction (Fig. 1*a*). SEM-EDX mapping on these clusters was used to investigate the chemical composition. From the EDX data quantitively two values were compared (Fig. 1*b-e*): the ratio of P/(Ca + Zn) to identify the occurrence of ion-exchange versus adsorption and the Zn/(Ca + Zn) which indicates the rate of ion-exchange. No drop in P/(Ca + Zn) ratio was measured suggesting that Ca is exchanged for Zn rather than the adsorption of Zn to the HAp exterior. Nevertheless, the P/(Ca + Zn) ratio increased, possibly indicating the introduction of cation hole defects. After 1 min exposure time, a Zn/(Ca + Zn) ratio of about 0.18 ± 0.068 could be obtained, implying that Zn ion-exchange has occurred replacing approximately 20 mol% of the Ca with Zn.

The influence of the procedure on crystallite shape was investigated using conventional TEM. This showed that nanometer-sized platelets were present both before and after the reaction (Fig. 1*g,h*), with a similar length (before 400 ± 138 nm, after 380 ± 171 nm) and width (before 170 ± 70 nm, after 170 ± 64 nm). The crystallinity was further probed by using Selective Area Electron Diffraction (SAED) measurements. No changes in diffraction spacings could be observed before and after ion-exchange, indicating that the crystalline structure remains intact (*insets of* Fig. 1 *g,h*). Note that, given the accuracy of the SAED measurements, this does not exclude that minor shifts in specific spacings might have occurred (*ESI section 1*).

To determine if the incorporation of Zn can be modulated by the exposure time to the $Zn(NO_3)_2$ solution, the reaction was repeated at 10 s, 15 min and 60 min. Again SEM-EDX measurements showed a slightly increased P/(Ca + Zn) value for all reaction times, indicating the predominant occurrence of ion-exchange over that of adsorption. With increasing reaction time, a Zn/(Ca + Zn) ratio of 0.16 ± 0.026 (10 s), 0.18 ± 0.068 (1 min), 0.17 ± 0.008 (15 min) and 0.22 ± 0.022 (60 min) was obtained (Fig. 1*f*). This shows that most of the ~ 15 mol% Zn is incorporated rapidly within the first

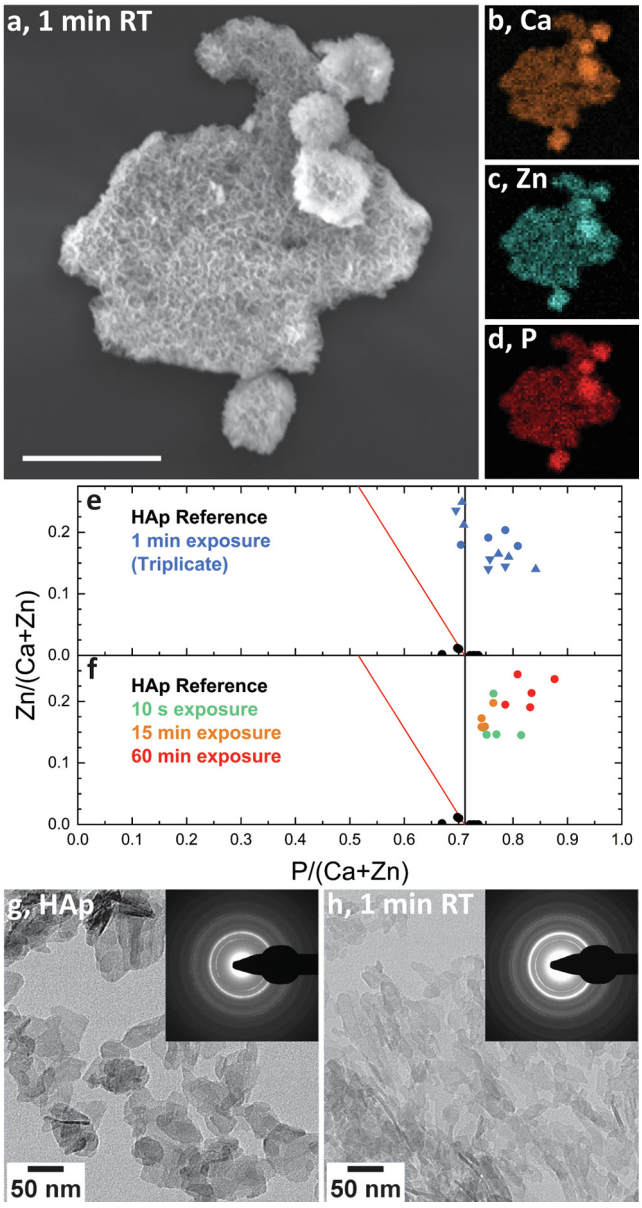

Fig. 1. SEM image of HAp clusters after exposure to 1 M $Zn(NO_3)_2$ solution (a, scale bar: 5 μm) and the corresponding EDX signals of Zn, Ca and P (b-d). Quantified EDX atomic ratios of Zn/(Ca + Zn) against P/(Ca + Zn) for apatite exposed to $ZnNO_3$ at RT for 1 min in triplicate (e, using a different symbol for each sample) and varying exposure time at RT (f). The black line corresponds to Ca - Zn ion-exchange, whereas the red line indicates maximum Zn adsorption to the HAp crystals. Conventional TEM images of as synthesized HAp (g) and after exposure to $Zn(NO_3)_2$ solution for 1 min (h); performed directly on a TEM grid. Inset: SEAD results of similar regions observed spacings; match with HAp (g-h). (For interpretation of the references to colour in this figure legend, the reader is referred to the web version of this article.)

10 s of exposure. After significantly increasing the exposure time to 60 min only a minor increase in the incorporated amount to ~ 22 mol% Zn can be achieved. This suggests that there is either a diffusion or ion-exchange barrier, preventing the incorporation of more Zn. Overall it shows that close to 20 mol% of Zn can be incorporated into HAp by exposure to $Zn(NO_3)_2$ under aqueous RT conditions, a result which is comparable to direct Zn-HAp synthesis.

3.2. Temperature effects

Generally, reaction and diffusion barriers can be overcome by elevating the reaction temperature. Therefore the experiments

were repeated at 53 °C using $Zn(NO_3)_2{\cdot}6H_2O$ solution concentrations of both 1 M and 2 M using either 1 min or 15 min exposure time (Fig. 2, *Experimental*). SEM-EDX studies after exposure showed that in all cases the Zn concentration in solution had no effect and therefore the given averages are combinations from both concentrations. EDX studies after 1 min ion-exchange at 53 °C showed a Zn/(Ca + Zn) ratio of 0.18 ± 0.02, similar to the value obtained at RT experiments. After 15 min reaction time, however, a strong increase in Zn/(Ca + Zn) ratio was observed to 0.44 ± 0.24. The P/(Ca + Zn) ratio showed a strong variation between 0.2 and 0.9. In most regions a measured increase in Zn/(Ca + Zn) ratio corresponded with a strong decrease in P/(Ca + Zn) ratio (Fig. 2), suggesting that adsorption of Zn is at least in part responsible for the relative increase in Zn. Notably multiple regions were identified that only had a minimal decrease in P/(Ca + Zn) ratio indicating minimal adsorption, while showing a Zn/(Ca + Zn) ratio as high as 0.8. TEM studies after ion-exchange further showed large populations of relatively small Zn-HAp crystals (*Fig. S1, 200* ± 79 nm by 80 ± 32 nm) compared to the original crystal (400 ± 138 nm by 170 ± 70 nm). This could indicate that the stress induced by Zn substitution induces cracking or that at elevated temperature dissolution of the Zn-HAp starts to occur. Performing the procedure at 80 °C only showed the incidental presence of particles (*Fig S2*), preventing further EDX studies. Overall, the data does suggest that a higher incorporation might be obtained, both by increasing exposure time and temperature. However, this is at a notable cost of uniformity throughout the sample, indicating full Zn incorporation may not be feasible.

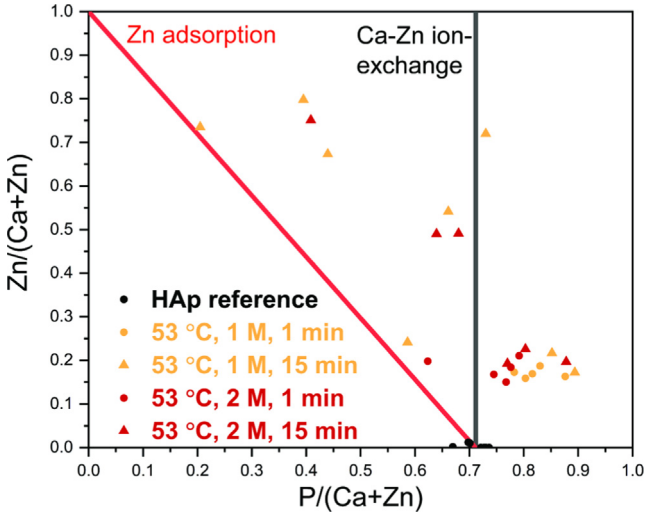

Fig. 2. Quantified EDX atomic ratios of Zn/(Ca + Zn) against P/(Ca + Zn) for apatite exposed to $ZnNO_3$ at 53 °C at varying concentrations and time.

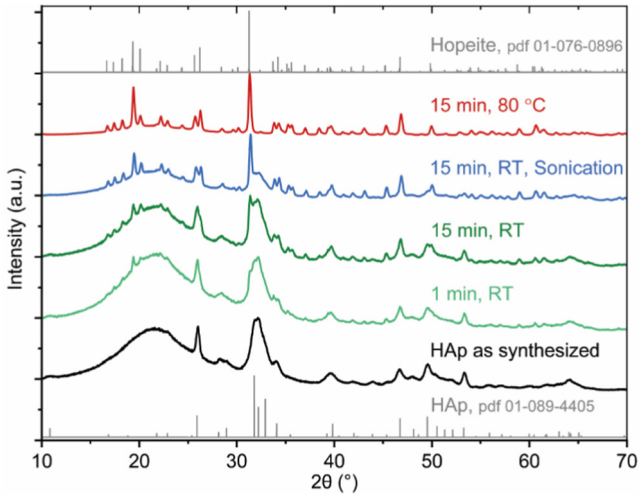

Fig. 3. pXRD pattern of HAp as synthesized (black) and HAp dispersed in 1 M Zn $(NO_3)_2{\cdot}6H_2O$ solution for 1 min at RT (light-green), 15 min at RT (dark-green), 15 min at RT while sonicating (blue) and 15 min at 80 °C (red). The broad pXRD signal visible at about 20° is due to the substrate. (For interpretation of the references to colour in this figure legend, the reader is referred to the web version of this article.)

3.3. Exchange of dispersed HAp crystals

To supplement on-grid studies, the exchange procedure was also performed on dispersed HAp crystals exposed for 15 min at 80 °C to a preheated 1 M $Zn(NO_3)_2{\cdot}6H_2O$ solution (*Experimental*). Powder X-Ray Diffraction (pXRD) of the purified product (Fig. 3) showed the dominant formation of hopeite with no (Zn-)HAp signals being identified. SEM studies on the product dominantly showed highly faceted micrometer-sized hopeite sheets with an ill-defined shape (Fig. 4*a-b*). The observation of hopeite is in sharp contrast with the incidentally observed HAp particles when using the on-grid procedure.

Further experiments on dispersed HAp crystals show that the formation of hopeite is not restricted to high temperature conditions. pXRD analysis of HAp exposed to a $Zn(NO_3)_2$ solution shows the presence of hopeite signals after as little as 1 min exposure time at RT (Fig. 3). These hopeite signals become more pronounced with increasing exposure time (15 min) and sonication. Upon sonication some minor changes in the pXRD pattern are observed. As the formation of hopeite is proceeding, adding energy (via sonication) might help and lead to a somewhat improved crystallinity. SEM studies (Fig. 4*c-d*) show, in contrast to the experiments performed at 80 °C, micrometer-sized sheets that are rectangular in shape, very similar to previously synthesized hopeite crystals by Parhi et al.[39] The sheets formed at RT are generally clean. Many of the hopeite sheets formed under sonication at RT are covered with small particles, presumably (Zn-)HAp. The presence of the latter could be due to better dispersion due to sonication.

3.4. Transformation to hopeite

There are two possible pathways for the transformation of Zn-HAp to hopeite. The first is the dissolution of Zn-HAp followed by reprecipitation into hopeite. A second route would be the direct transformation into hopeite. The initial nanometer-sized Zn-HAp crystals are significantly smaller than the formed micrometer-sized hopeite crystals, which is highly unusual for a direct transformation strategy. Furthermore, hopeite crystals were not observed when using the on-grid exchange procedure although their presence would be expected for a direct transformation. Given that the grids are floated on or suspended in the $Zn(NO_3)_2$ solution (*Fig. S3*), dissolution and recrystallization to hopeite probably predominantly takes place in the solution phase with the crystals subsequently sedimenting in the liquid phase, a process matching observations. This leaves dissolution and reprecipitation as the most likely mechanism.

A dissolution reprecipitation mechanism, however, does not preclude local interaction between hopeite and Zn-HAp crystals. It is possible that local dissolution of the Zn-HAp crystals is required for the formation of the large hopeite sheets. Indeed, using conventional TEM on the powder sample formed at 15 min at RT showed Zn-HAp crystals aggregated on hopeite crystals. Specifically, not well developed crystal facets were covered with Zn-HAp crystals (Fig. 5). One suggestion is that the dissolution reprecipitation process occurs locally. Unfortunately, the hopeite

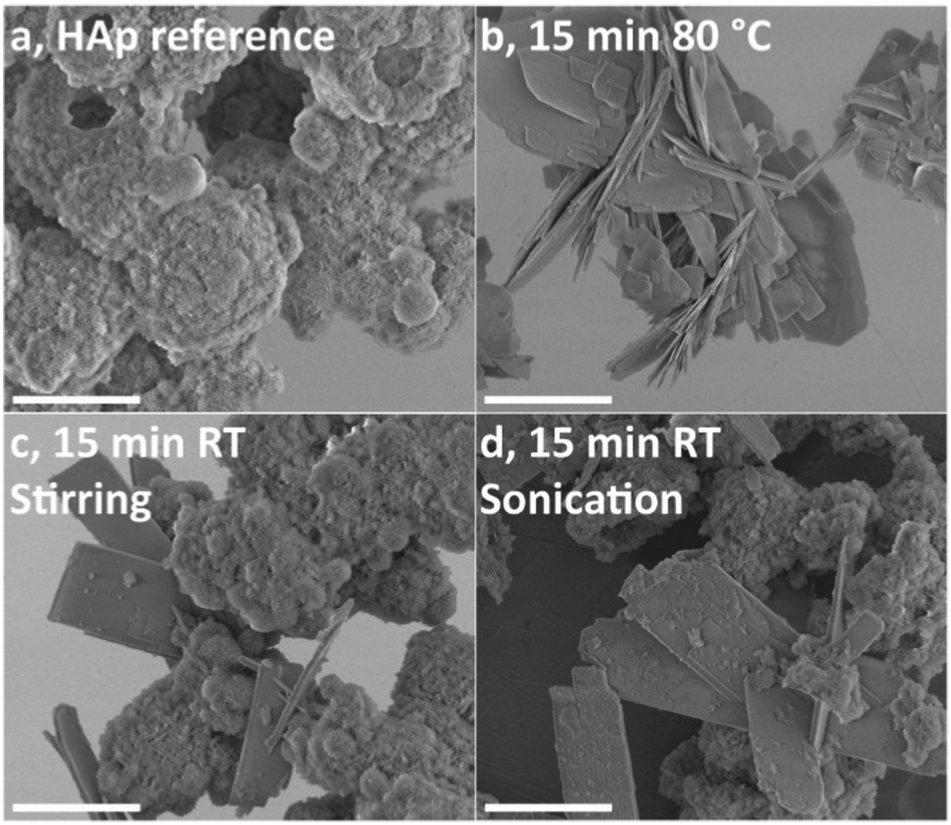

Fig. 4. SEM images of HAp before ion-exchange (a) and Zn-HAp and Hopeite crystals obtained after HAp exposure to 1 M $Zn(NO_3)_2.6H_2O$ solution at pH 2.7 for 15 min at 80 °C (b), 15 min stirring at RT (c), and 15 min sonication at RT (d). Scale bar: 10 μm.

crystals proved too thick for cryoTEM imaging, preventing the time-resolved studies of their formation *in-situ*. This makes it unclear whether these Zn-HAp filled defects are due to drying effects, the presence of Zn-HAp or a local mineralization process.

Parhi et al.[39] demonstrated that, at low pH, hopeite can be synthesized in water at room temperature by mixing ZnCl and sodium phosphate solutions. This suggests that, if Zn and PO_4^{3-} ions are present in solution, hopeite is the preferred crystallization product although not necessarily the thermodynamically most stable one. Therefore, to identify whether the formation of hopeite at higher reaction temperatures is a simple dissolution and reprecipitation process caused by the natural dissolution of HAp under these conditions, a control experiment at 80 °C at pH 2.7 in the absence of Zn was performed. After the reaction a significant amount of white powder was collected. pXRD and TEM studies (*Fig. S4*) showed the presence of pure HAp crystals. This demonstrates that Zn is essential for the dissolution process.

Previously mentioned EDX studies show that roughly 20 mol% of the Ca can be exchanged with Zn. Since the spatial resolution of SEM EDX analysis is limited it cannot distinguish between ions present on the surface or throughout the crystal. The HAp crystals investigated have a thickness of about 4.2 ± 0.69 nm based on measurements on tilted crystals observed by cryoTEM (*Fig. S5*). A HAp unit cell has a *c*-axis of ~ 7 Å,[40] meaning a single crystal is ~ 6 unit cells in thickness. If 20 mol% of the Ca in HAp is exchanged with Zn in a surface layer, this would give a layer thickness of ~ ½ a unit cell on either side. To support such an assumption, a value of the diffusion constant of Zn in HAp would be helpful. However, direct data are absent and given the broad range of experimentally determined activation energies for other ions which do not uniquely relate to the ionic radius, it also appeared to be unfeasible to reliably estimate the diffusion constant of Zn into apatite.[41,42]

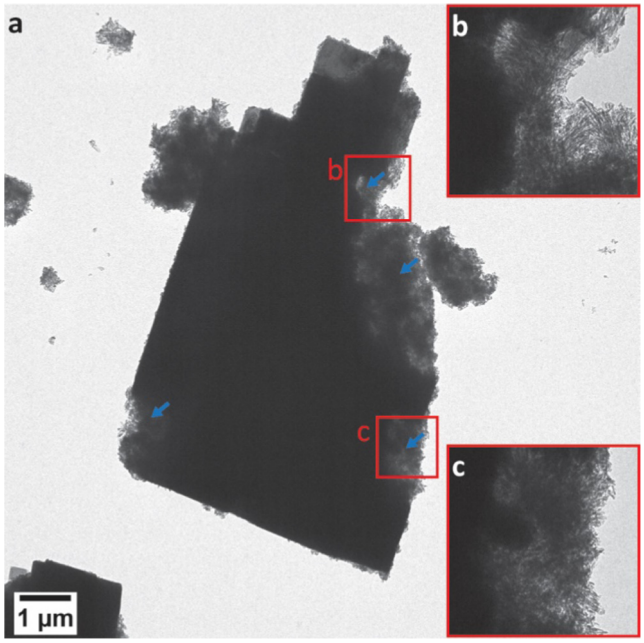

Fig. 5. Conventional TEM image (a) of a hopeite crystal with Zn-HAp crystals in observed crystal defects (blue arrows) in a 15 min RT experiments. Higher magnification insets (b-c) of hopeite Zn-HAp interface regions. (For interpretation of the references to colour in this figure legend, the reader is referred to the web version of this article.)

Hence it is not realistic to determine the positioning of Zn throughout the Zn-HAp crystals based on experimental evidence or calcu-

lations. Therefore, to gain more insight the results were compared to existing literature.

In literature, using direct synthesis, a HAp exchange limit of ~ 20 mol% Ca with Zn was obtained, the distribution of which is expected to be homogeneous. Furthermore, increasing the Zn fraction above 20 mol% during synthesis results in increased amounts of hopeite. In addition, performing ion-exchange with a range of cations in organic solvents, a similar degree of cation incorporation was achieved by Chen et al.[38] These observations combined with the results from the current work suggest that the Zn is homogeneously distributed throughout the crystal. This indicates that the incorporation of Zn into HAp is limited to about 20 mol%. The ionic radius of Zn (0.88 Å) is smaller than of Ca (1.14 Å)[43]. Incorporating Zn therefore results in internal stress in the crystal. If the crystal is unable to reconfigure to release this stress, its stability decreases, and, when in contact with water, possibly resulting in dissolution eventually. Calculations by Flora et al. [20] indicate that fully converted Zn-HAp ($Zn_{10}(PO_4)_6(OH)_2$) has a negative Gibbs energy of dissolution, matching our inference. This would mean that hopeite is not only formed because it is the most preferred crystal at this low pH and Zn-rich conditions, but that the Zn-HAp is simply too unstable to exist under the experimental conditions. It also means that it is highly unlikely that a higher degree of Zn incorporation in Zn-HAp can be achieved in absence of any stabilization agents in water.

4. Conclusion

Exposing HAp to a simple aqueous ion-exchange strategy, up to ~ 20 mol% of the Ca atoms could consistently be replaced with Zn atoms without influencing the morphology or crystallinity. The initial exchange with Zn occurs rapidly reaching ~ 16 mol% exchange within seconds. A larger amount of Zn could be incorporated with increasing reaction time (up to 22 mol% after 60 min) or by elevating the reaction temperature (incidental high conversion). The incorporation of Zn decreases the stability of the resulting Zn-HAp, resulting in an increased dissolution of these crystals and reprecipitation into hopeite crystals with increasing Zn incorporation. The limited stability of the Zn-HAp crystals under aqueous conditions in the absence of stabilization agents, therefore, does not permit the homogenous formation of a more Zn-rich Zn-HAp. However, the method used leads to the rapid incorporation of the maximum amount of Zn in HAp without destabilizing the lattice.

Funding

This project was partially funded by a TopPunt grant (Bi-Hy, 718.016.003) of the Dutch Research Council (NWO).

Declaration of Competing Interest

The authors declare that they have no known competing financial interests or personal relationships that could have appeared to influence the work reported in this paper.

Acknowledgements

The authors would like to thank Prof. Nico A. J. M. Sommerdijk (Radboud UMC, Nijmegen) for his contribution during the initial stages of this work.

Data availability

The raw and processed data required to reproduce these findings cannot be shared at this time as the data also forms part of an ongoing study.

Appendix A. Supplementary data

Supplementary data to this article can be found online at https://doi.org/10.1016/j.matdes.2021.109846.

References

[1] M. Pandya, T.G.H. Diekwisch, Enamel Biomimetics-fiction or Future of Dentistry, Int. J. Oral Sci. 11 (2019) 8.
[2] Y. Liu, D. Luo, T. Wang, Hierarchical Structures of Bone and Bioinspired Bone Tissue Engineering, Small 12 (34) (2016) 4611–4632.
[3] M.K. Islam, P.J. Hazell, J.P. Escobedo, H. Wang, Biomimetic armour design strategies for additive manufacturing: A review, Mater Design 205 (2021) 109730.
[4] W.J. Habraken, J. Tao, L.J. Brylka, H. Friedrich, L. Bertinetti, A.S. Schenk, A. Verch, V. Dmitrovic, P.H. Bomans, P.M. Frederik, J. Laven, P. van der Schoot, B. Aichmayer, G. de With, J.J. DeYoreo, N.A. Sommerdijk, Ion-association Complexes Unite Classical and Non-classical Theories for the Biomimetic Nucleation of Calcium Phosphate, Nat. Commun. 4 (2013) 1507.
[5] L.C. Bonar, A.H. Roufosse, W.K. Sabine, M.D. Grynpas, M.J. Glimcher, X-Ray-Diffraction Studies of the Crystallinity of Bone-Mineral in Newly Synthesized and Density Fractionated Bone, Calcified Tissue Int 35 (2) (1983) 202–209.
[6] F. Nudelman, K. Pieterse, A. George, P.H.H. Bomans, H. Friedrich, L.J. Brylka, P.A. J. Hilbers, G. de With, N.A.J.M. Sommerdijk, The Role of Collagen in Bone Apatite Formation in the Presence of Hydroxyapatite Nucleation Inhibitors, Nat. Mater. 9 (2010) 1004–1009.
[7] B.M. Oosterlaken, M.P. Vena, G. de With, In Vitro Mineralization of Collagen, Adv. Mater. 2004418 (2021).
[8] H. Ping, H. Xie, Y.M. Wan, Z.X. Zhang, J. Zhang, M.Y. Xiang, J.J. Xie, H. Wang, W. M. Wang, Z.Y. Fu, Confinement Controlled Mineralization of Calcium Carbonate within Collagen Fibrils, J. Mater. Chem. B 4 (5) (2016) 880–886.
[9] L.N. Niu, K. Jiao, H. Ryou, A. Diogenes, C.K.Y. Yiu, A. Mazzoni, J.H. Chen, D.D. Arola, K.M. Hargreaves, D.H. Pashley, F.R. Tay, Biomimetic Silicification of Demineralized Hierarchical Collagenous Tissues, Biomacromolecules 14 (5) (2013) 1661–1668.
[10] B. Zhou, L.N. Niu, W. Shi, W. Zhang, D.D. Arola, L. Breschi, J. Mao, J.H. Chen, D.H. Pashley, F.R. Tay, Adopting the Principles of Collagen Biomineralization for Intrafibrillar Infiltration of Yttria-Stabilized Zirconia into Three-Dimensional Collagen Scaffolds, Adv. Funct. Mater. 24 (13) (2014) 1895–1903.
[11] Y. Xu, F. Nudelman, E.D. Eren, M.J.M. Wirix, B. Cantaert, W.H. Nijhuis, D. Hermida-Merino, G. Portale, P.H.H. Bomans, C. Ottmann, H. Friedrich, W. Bras, A. Akiva, J.P.R.O. Orgel, F.C. Meldrum, N. Sommerdijk, Intermolecular Channels Direct Crystal Orientation in Mineralized Collagen, Nat. Commun. 11 (1) (2020) 5068.
[12] M.D. Wadge, B.W. Stuart, K.G. Thomas, D.M. Grant, Generation and characterisation of gallium titanate surfaces through hydrothermal ion-exchange processes, Mater Design 155 (2018) 264–277.
[13] L. De Trizio, L. Manna, Forging Colloidal Nanostructures via Cation Exchange Reactions, Chem. Rev. 116 (18) (2016) 10852–10887.
[14] T. Holtus, L. Helmbrecht, H.C. Hendrikse, I. Baglai, S. Meuret, G.W.P. Adhyaksa, E.C. Garnett, W.L. Noorduin, Shape-preserving Transformation of Carbonate Minerals into Lead Halide Perovskite Semiconductors based on Ion Exchange/Insertion Reactions, Nat. Chem. 10 (7) (2018) 740–745.
[15] T.R. Bian, K. Zhao, Q.N. Meng, Y.F. Tang, H. Jiao, J. Luo, The construction and performance of multi-level hierarchical hydroxyapatite (HA)/collagen composite implant based on biomimetic bone Haversian motif, Mater Design 162 (2019) 60–69.
[16] K.M. Conway, C. Kunka, B.C. White, G.J. Pataky, B.L. Boyce, Increasing fracture toughness via architected porosity, Mater Design 205 (2021) 109696.
[17] A. Mushtaq, R.B. Zhao, D.D. Luo, E. Dempsey, X.M. Wang, M.Z. Iqbal, X.D. Kong, Magnetic hydroxyapatite nanocomposites: The advances from synthesis to biomedical applications, Mater Design 197 (2021).
[18] S.J. Omelon, M.D. Grynpas, Relationships between Polyphosphate Chemistry, Biochemistry and Apatite Biomineralization, Chem. Rev. 108 (11) (2008) 4694–4715.
[19] D.J. Zhang, A. Tamilselvan, Lattice Energy and Mechanical Stiffness of Hydroxyapatite, J Mater Sci-Mater M 18 (1) (2007) 79–87.
[20] N.J. Flora, C.H. Yoder, H.D.B. Jenkins, Lattice Energies of Apatites and the Estimation of ΔH-f°(PO4(3-), g), Inorg. Chem. 43 (7) (2004) 2340–2345.
[21] L. Glasser, H.D.B. Jenkins, Lattice Energies and Unit Cell Volumes of Complex Ionic Solids, J. Am. Chem. Soc. 122 (4) (2000) 632–638.
[22] R. Sergi, D. Bellucci, R.T. Candidato, L. Lusvarghi, G. Bolelli, L. Pawlowski, G. Candiani, L. Altomare, L. De Nardo, V. Cannillo, Bioactive Zn-doped Hydroxyapatite Coatings and their Antibacterial Efficacy against Escherichia Coli and Staphylococcus Aureus, Surf Coat Tech 352 (2018) 84–91.
[23] L. Robinson, K. Salma-Ancane, L. Stipniece, B.J. Meenan, A.R. Boyd, The Deposition of Strontium and Zinc Co-substituted Hydroxyapatite Coatings, J Mater Sci-Mater M 28 (3) (2017) 51.
[24] R. Rogojan, E. Andronescu, M. Necula, C. Cercel, R. Popescu, G. Stoian, Calcium Phosphate Nanoparticles Substituted with Zn2+/Cu2+ - as Antibacterial Systems, Rom Biotech Lett 23 (2) (2018) 13425–13438.
[25] J.R. Guerra-Lopez, G.A. Echeverria, J.A. Guida, R. Vina, G. Punte, Synthetic Hydroxyapatites Doped with Zn(II) Studied by X-ray Diffraction, Infrared, Raman and Thermal Analysis, J. Phys. Chem. Solids 81 (2015) 57–65.

[26] H. Kim, S. Mondal, S. Bharathiraja, P. Manivasagan, M.S. Moorthy, J. Oh, Optimized Zn-doped Hydroxyapatite/Doxorubicin Bioceramics System for Efficient Drug Delivery and Tissue Engineering Application, Ceram. Int. 44 (6) (2018) 6062–6071.
[27] C. Kojima, K. Watanabe, H. Murata, Y. Nishio, R. Makiura, K. Matsunaga, A. Nakahira, Controlled Release of DNA from Zinc and Magnesium Ion-doped Hydroxyapatites, Res Chem Intermediat 45 (1) (2019) 23–32.
[28] M.O. Li, X.F. Xiao, R.F. Liu, C.Y. Chen, L.Z. Huang, Structural Characterization of Zinc-substituted Hydroxyapatite Prepared by Hydrothermal Method, J Mater Sci-Mater M 19 (2) (2008) 797–803.
[29] G.L. Meng, X.L. Wu, R.J. Yao, J. He, W. Yao, F. Wu, Effect of Zinc Substitution in Hydroxyapatite Coating on Osteoblast and Osteoclast Differentiation under Osteoblast/Osteoclast Co-culture, Regen Biomater 6 (6) (2019) 349–359.
[30] N. Lowry, M. Brolly, Y. Han, S. McKillop, B.J. Meenan, A.R. Boyd, Synthesis and Characterisation of Nanophase Hydroxyapatite Co-substituted with Strontium and Zinc, Ceram. Int. 44 (7) (2018) 7761–7770.
[31] S. Hayakawa, K. Ando, K. Tsuru, A. Osaka, E. Fujii, K. Kawabata, C. Bonhomme, F. Babonneau, Structural Characterization and Protein Adsorption Property of Hydroxyapatite Particles Modified with Zinc Ions, J. Am. Ceram. Soc. 90 (2) (2007) 565–569.
[32] E. Fujii, M. Ohkubo, K. Tsuru, S. Hayakawa, A. Osaka, K. Kawabata, C. Bonhomme, F. Babonneau, Selective Protein Adsorption Property and Characterization of Nano-crystalline Zinc-containing Hydroxyapatite, Acta Biomater. 2 (1) (2006) 69–74.
[33] X. Zhao, Y. Zhu, Z. Zhu, Y. Liang, Y. Niu, J. Lin, Characterization, Dissolution, and Solubility of Zn-Substituted Hydroxylapatites [(ZnxCa1−x)5(PO4)3OH] at 25°C, J. Chem. 2017 (2017) 1–13.
[34] F.Z. Ren, R.L. Xin, X. Ge, Y. Leng, Characterization and Structural Analysis of Zinc-substituted Hydroxyapatites, Acta Biomater. 5 (8) (2009) 3141–3149.
[35] F. Miyaji, Y. Kono, Y. Suyama, Formation and Structure of Zinc-substituted Calcium Hydroxyapatite, MRS Bull. 40 (2) (2005) 209–220.
[36] J. Oliva, J. De Pablo, J.L. Cortina, J. Cama, C. Ayora, The use of Apatite II (TM) to Remove Divalent Metal Ions Zinc(II), Lead(II), Manganese(II) and Iron(II) from Water in Passive Treatment Systems: Column Experiments, J. Hazard. Mater. 184 (1–3) (2010) 364–374.
[37] Q. Wang, P.F. Tang, X. Ge, P.F. Li, C. Lv, M.H. Wang, K.F. Wang, L.M. Fang, X. Lu, Experimental and Simulation Studies of Strontium/Zinc-codoped Hydroxyapatite Porous Scaffolds with Excellent Osteoinductivity and Antibacterial Activity, Appl. Surf. Sci. 462 (2018) 118–126.
[38] G.Y. Chen, X.Y. Zheng, C. Wang, J.F. Hui, X.X. Sheng, X.X. Xu, J.C. Bao, W.J. Xiu, L. H. Yuwen, D.D. Fan, A Postsynthetic Ion Exchange Method for Tunable Doping of Hydroxyapatite Nanocrystals, RSC Adv. 7 (89) (2017) 56537–56542.
[39] P. Parhi, V. Manivannan, S. Kohli, P. McCurdy, Room Temperature Metathetic Synthesis and Characterization of Alpha-hopeite, Zn-3(PO4)(2)·4H(2)O, MRS Bull. 43 (7) (2008) 1836–1841.
[40] J.C. Elliott, R.M. Wilson, S.E.P. Dowker, Apatite Structures, Adv. X-Ray Anal. 45 (2002) 172–181.
[41] D.J. Cherniak, W.A. Lanford, F.J. Ryerson, Lead Diffusion in Apatite and Zircon Using Ion-Implantation and Rutherford Backscattering Techniques, Geochim. Cosmochim. Acta 55 (6) (1991) 1663–1673.
[42] D.J. Cherniak, Uranium and Manganese Diffusion in Apatite, Chem. Geol. 219 (1–4) (2005) 297–308.
[43] R.D. Shannon, Revised Effective Ionic-Radii and Systematic Studies of Interatomic Distances in Halides and Chalcogenides, Acta Crystallographica Section A 32 (Sep1) (1976) 751–767.